



Mechanisms of micro-groove formation on single-crystal diamond by a nanosecond pulsed laser

Nozomi Takayama, Jiwang Yan*

Department of Mechanical Engineering, Keio University, Hiyoshi 3-14-1, Kohoku, Yokohama, Kanagawa 223-8522, Japan



ARTICLE INFO

Article history:

Received 22 July 2016

Received in revised form

25 December 2016

Accepted 31 December 2016

Available online 31 December 2016

Keywords:

Nd:YAG laser

Laser processing

Micromachining

Single-crystal diamond

Thermal ablation

Groove formation

Surface microstructure

ABSTRACT

Micro-grooves were machined onto a single-crystal diamond surface by laser irradiation with a nanosecond pulse, and the resulting damage was investigated. The causes of four different forms of damage have been identified and examined; cracking, ripple formation, groove shape deformation and debris deposition. Cracking is caused by a rapid temperature change; ripples by interference of the laser reflected from the groove walls; groove shape deformation by enhanced absorption of the laser-induced plasma; deposited ablation debris by two different ablation regimes. Cracking and shape deformation is reduced at the center of the groove, which is very smooth and ripple-free for line irradiations using a single pass. These results provide useful information for reducing the laser-induced damage in diamond and creating damage-free micro-grooved diamond cutting tools.

© 2016 Elsevier B.V. All rights reserved.

1. Introduction

Micro-grooves have become an increasingly significant surface microstructure in a wide range of fields, especially in bio-medical science. Micro-grooves have been shown to cause cell alignment (Wilkinson et al., 2002), enabling the growth of well-orientated cells for use in tissue repair. Moreover, Korin et al. (2009) have shown that they may protect sensitive cells from the detrimental effects of fluidic shear stress and thus enable the cultivation of sensitive cells. Furthermore, Frenkel et al. (2002) have presented machining of micro-grooves onto the surface of implants (such as joint replacements) as a method to improve osseointegration and thus to lengthen implant life span. Micro-grooves are a highly useful surface texture but they are difficult to machine on specific kinds of materials. Micro-grooves are conventionally processed by photolithography which has given rise to problems such as limited groove geometry, accuracy and usable materials. Laser machining involving the direct irradiation of grooves into a metal surface has also been attempted, but Fasasi et al. (2009) have demonstrated a few problems including groove wall deformation and re-solidification pockets due to melting, as well as a large heat affected zone (HAZ). Alternatively, cutting micro-grooves on metals with a diamond tool is not only more accurate but is also able to

reduce the thermal effect compared to laser machining (Yan et al., 2009).

Fabricating micro-grooves on the surface of a diamond tool is also very important. Previous studies have shown that processing micro-grooves onto the rake face of a cutting tool can be effective in improving cutting fluid retention of the tool surface (Sugihara and Enomoto, 2009), reducing the friction force (Obikawa et al., 2011) and the required cutting force (Kawasegi et al., 2009). However, there have not yet been many attempts to make micro-grooves on the cutting edge of a tool. By grooving the cutting edge of tools, it becomes possible to transfer the edge shape onto the substrate surface. The grooved tools can be used to transfer the micro-grooves onto metal materials, making the machining of micro-grooves much more rapid, precise and without burr formation. Unlike the direct fabrication of micro-grooves on metal by laser irradiation, the wall deformation and re-solidification pockets due to melting are not of much concern in the cutting process with a diamond tool.

It is possible to create such a micro-grooved tool using laser irradiation. It is known that diamond transforms into graphite and is ablated by laser pulses. However, it is important to determine the optimal laser parameters in tool processing so as to avoid the generation of a HAZ and subsurface damage (SSD). Eberle et al. (2015) have stated that the HAZ and SSD will cause the tool to exhibit reduced performance, reduced tool life, reduced wear resistance and greater required cutting force.

The laser machining of diamond has been a subject of great interest for the past several decades. Previous studies have estab-

* Corresponding author.

E-mail address: yan@mech.keio.ac.jp (J. Yan).

lished that a femtosecond pulsed laser is more suitable for precision manufacture of extremely small surface structures compared to a longer pulse, as they allow for the use of lower photon energies without loss of precision (Dumitru et al., 2002) or spatial resolution (Preuss and Stuke, 1995). Chichkov et al. (1996) have shown that sharp, well-defined (in other words, damage-free) patterns can be ablated. This is due to the reduced thermal effects of an ultra-fast pulse; strong electrostatic ion repulsion force causes break-up of di-electric surfaces, accounting for the nonthermal nature. Furthermore, Stuart et al. (1996) have demonstrated that the ablation threshold is lower for a femtosecond pulsed laser. However, processing costs for a femtosecond laser are much higher and the material removal rate much lower than for a nanosecond laser, especially when machining a deep groove or a large-size structure, like a cutting tool. Thus, to create a micro-grooved tool, a nanosecond pulse would be more appropriate if used along with a damage prevention method. Previous studies discussing the nanosecond laser irradiation of diamond have focused on developing an ablation model (Rothschild et al., 1986), where surface graphitization of diamond is followed by sublimation or reaction. Konov (2012) has reported on the relation between ablation rate and laser fluence and Kononenko et al. (2005) have discussed the laser-induced graphitization of diamond. Despite extensive research on nanosecond pulsed irradiation on diamond, the formation mechanism of the laser-induced damage and the conditions for reducing the damage have not been clarified. Hence, it is important to further address this issue in order to develop methods to prevent damage during nanosecond pulsed irradiation. The ultimate aim of this study is to develop a damage-free method to machine micro-grooves and other micro-structures into diamond to fabricate high-performance cutting tools.

2. Experimental method

The laser used in the following experiments was LR-SHG, a Nd:YAG laser pumped by LD, from MegaOpto Co., Ltd. It has a maximum power output of >1W and a pulse width of 15.6 ns at 1 kHz, a wavelength of 532 nm and a spot diameter of 85 μm . For the following experiments, a pulse frequency of 1 kHz was used. The laser output energy has an approximate Gaussian distribution. The laser was controlled using a galvanometer scanner system with a Miramo controller made by YE Data Inc. Laser motion programs were created using GmcLib.DLL 2.0 software and FFFTP software was used to download these programs to the galvanometer scanner system. The laser beam was focused onto a stage using an f0 lens. The diamond used was prepared by chemical vapor deposition (CVD) in rectangular samples with dimensions of $4 \times 3.5 \times 1.12 \pm 0.02$ mm. The surfaces were flat and polished. The irradiated surface was the (100) Miller surface. All the other faces also had an equivalent crystal orientation. The groove depth was measured using the MP-3 laser probe made by Mitaka Kohki Co., Ltd. And the surface structure was observed by the Inspect S50 Scanning Electron Microscope (SEM) made by FEI Company. The atomic structure was identified by a Raman spectrometer (NRS-3100 by JASCO Corporation).

The diamond sample was placed on a base with an opening so that the lower surface was not in contact with the stage surface, as indicated in Fig. 1. As diamond is a transparent material at the laser wavelength used, when the diamond was placed directly onto the stage, the laser energy was absorbed by the stage surface, leaving an irradiation mark on the stage. The heat accumulated by the stage then affected and machined the diamond, also leaving an irradiation mark on the lower surface of diamond. In this case, the laser cannot directly machine the diamond and no meaningful results would be obtained. By using the base, no irradiation marks was

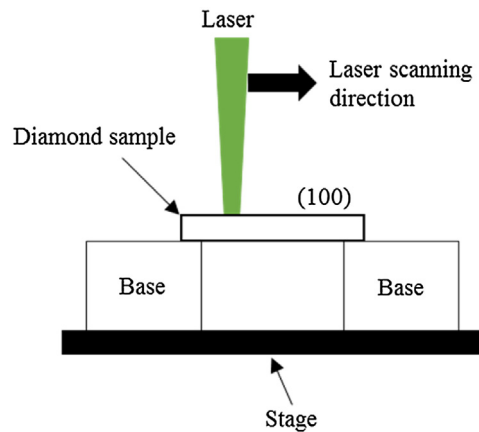


Fig. 1. Laser irradiation schematic for micro-grooving on diamond.

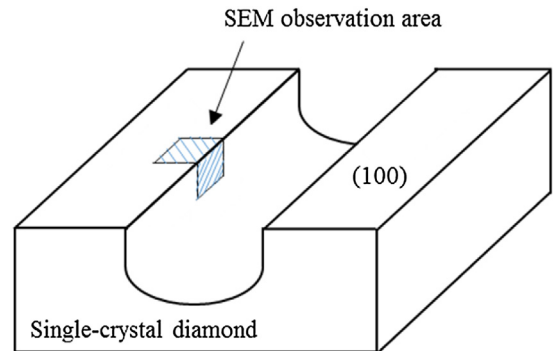


Fig. 2. Schematic of SEM observation area on the groove formed by laser irradiation.

produced on the stage or lower diamond surface, showing that the heat absorbed by the stage would not affect the diamond. Line irradiations, 300 μm in length, were performed at a constant scanning speed of 2 mm/s. These line irradiations were first performed with varying laser fluence. Laser fluence was changed in the range of 5.0–8.4 J/cm^2 . A lower boundary of 5.0 J/cm^2 was chosen as an even lower fluence of 4.2 J/cm^2 did not produce a clear groove. The lowest fluence was chosen for all the subsequent experiments as it produced the least cracking. The number of passes (or the number of times the line irradiation was repeated) was varied in the range of 2–60 passes. The irradiated surfaces were covered in debris so they were cleaned by being placed in a solution of nitric, sulphuric and perchloric acid (in a volume ratio of roughly 1:5:3) and heated to $\sim 200^\circ\text{C}$. This cleaning process removed the debris and was performed before SEM and laser probe observations.

3. Results and discussion

3.1. Cracking behavior

Many cracks were observed on the irradiated surfaces. The schematic for SEM observation is illustrated in Fig. 2. Different sized cracks were formed depending on the laser fluence. As shown in Fig. 3a-d, the cracking region size increased with increasing laser fluence. Upon closer examination, 2 different types of cracks were visible. First, as presented in Fig. 4a, there was a region of wide, open cracks near the groove edge. Second, as shown in Fig. 4b, there were thin straight cracks closer to the center. At the lowest fluence of 5.0 J/cm^2 , no open cracks were visible; instead, there were thin, bent cracks near the groove edge. It appeared that these cracks were similar in structure to the wide, open cracks due to their position and their lack of straightness. Furthermore, as presented

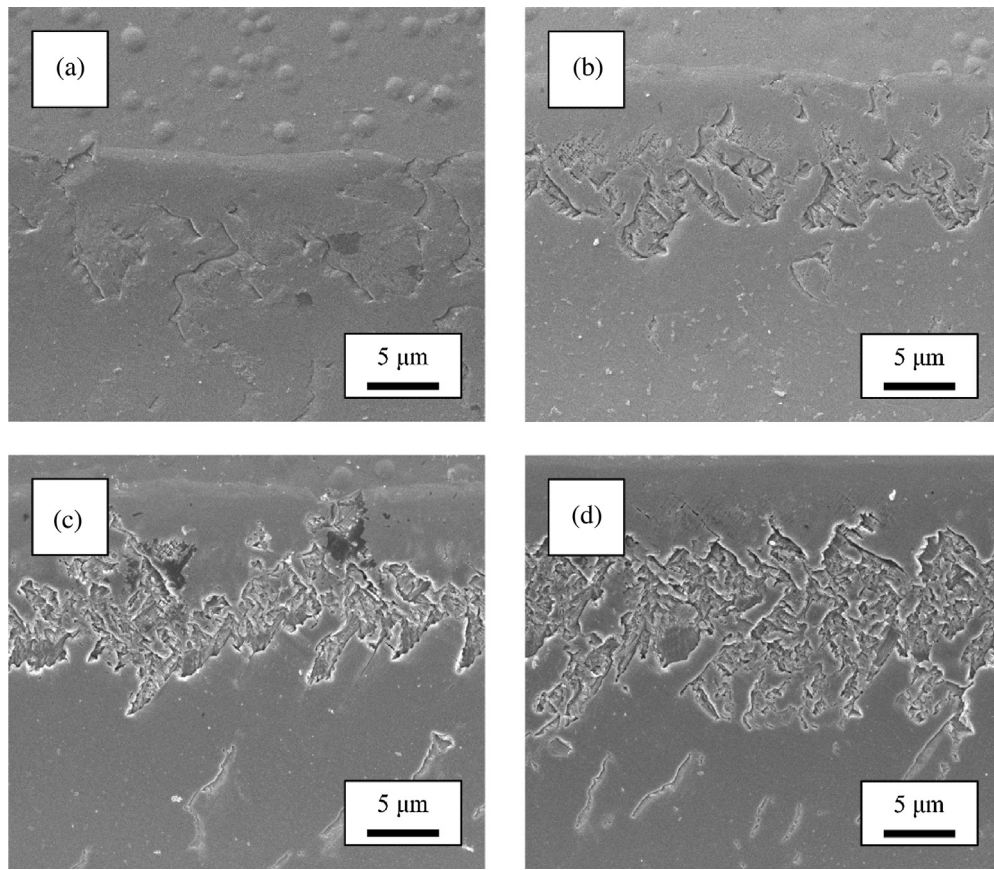


Fig. 3. SEM images of cracks formed near the edge of the groove when using a laser fluence of: (a) 5.0, (b) 6.0, (c) 7.2, (d) 8.4 J/cm².

in Fig. 4c, there was a smoothed, crack-free region in the center of each groove. The difference between the 2 different crack types can be explained by looking at the depth that they exist. The wider open cracks occur at a shallower depth of $\sim 1 \mu\text{m}$. These open cracks are easily propagated over a large area even with a low laser fluence. Crack propagation is facilitated by the existence of a near-surface defect layer that is formed during polishing. Therefore, despite the surface appearing to be damage-free, it is likely that a $\sim 1 \mu\text{m}$ layer of pits, scratches and potential micro-cracks exists under the polished surface as shown by Lee (2011). The thinner cracks seen in the groove produced by irradiation using 8.4 J/cm^2 laser fluence, most likely originated from deeper, smaller defects, and thus require a greater laser fluence to be propagated.

Here, it is necessary to understand the mechanism behind crack propagation. As diamond is not a good absorber (theoretically speaking, it is a transparent material at the wavelength used), Bloembergen (1973) showed that laser absorption is initiated from the near-surface defects such as cracks, pores and impurity inclusions. Moreover, Feit and Rubenchik (2004) showed that cracks typically contain nano-absorbers, such as polishing slurry and absorbing particles attracted by dangling bonds, which are able to absorb the laser energy. The energy absorbed generates high temperatures in absorbing areas within the laser spot. This temperature increase ΔT , between the initial sample temperature and the maximum temperature induced during laser irradiation, leads to a high triaxial stress S :

$$S = \frac{\alpha E \Delta T}{1 - 2\nu} \quad (1)$$

where α is the thermal expansion coefficient, E is the Young's modulus of elasticity and ν is Poisson's ratio. As the laser energy has a Gaussian distribution, ΔT and S depends on the distance from

the spot center. Brittle materials are susceptible to catastrophic fracture under conditions of large temperature changes induced by laser irradiation (Johansen et al., 1995). The crack propagation can be described in the following mechanical model presented by Hasselman (1969). The material is assumed to be entirely brittle and to contain mechanical flaws in the form of Griffith micro-cracks. The total energy W_t per unit volume is the sum of elastic energy and the cracks' fracture energy. Assuming that the cracks are penny-shaped, the total energy is described in the following equation:

$$W_t = \frac{3(\alpha \Delta T)^2 E_0}{2(1-2\nu)} \left[1 + \frac{16(1-\nu^2)Nl^3}{(1-2\nu)} \right] + 2\pi Nl^2 \quad (2)$$

where E_0 is the Young's modulus of the crack-free material, l is the crack length and N is the number of cracks per unit volume. The crack instability condition is:

$$\frac{dW_t}{dl} = 0 \quad (3)$$

Beyond this minimum value, the crack length is shown to increase with ΔT . A greater laser fluence leads to greater absorbed energy and a greater temperature change. Therefore, longer cracks are produced when using a greater laser fluence. The SEM images of Fig. 3 agrees with this, where larger cracks were found at higher fluences.

In addition, as presented by Sack (1946), critical fracture stress (the minimum stress required to initiate fracture) S_t for a penny-shaped crack can be written in the following way, given that G is the strain energy release rate:

$$S_t = \left[\frac{GE_0}{2(1-\nu^2)l_0} \right]^{\frac{1}{2}} \quad (4)$$

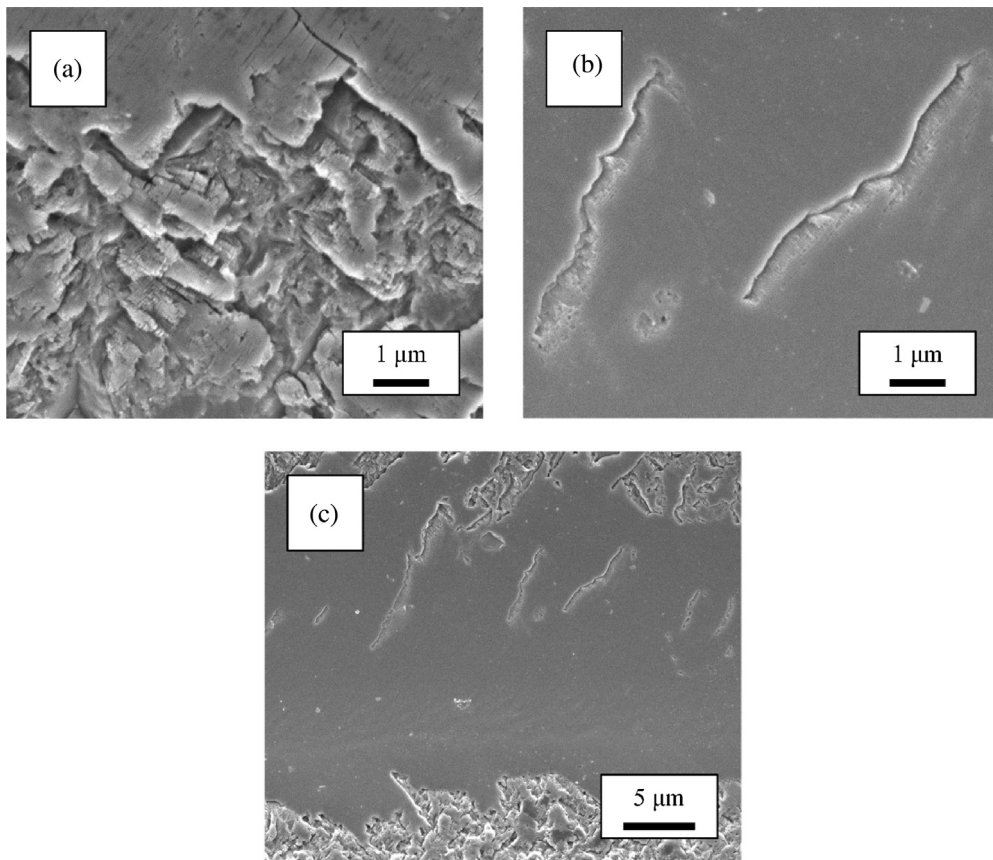


Fig. 4. Closer examination by SEM of cracks formed near the edge of the groove using a laser fluence of 8.4 J/cm^2 showed: (a) large area cracks, (b) thin cracks, (c) a smooth region in the center of the groove.

When the initial crack length l_0 is small, the fracture stress is larger. This explains why the thin cracks, which were initially not visible, were not propagated at a low laser fluence. Lower fluences could not induce high enough temperatures and thus stress to cause propagation of thin cracks.

The cracks and smooth region were further considered by measuring the cross-section profiles of the grooves and the results are shown in Fig. 5. The intensity at the edge of the groove is the ablation threshold. This is followed by a region of cracking and then a smooth region exists in the center. Therefore, smoothing effects occur at a higher fluence than cracking. Within the cracking region, the crack propagation depth is greater than the ablation depth. Therefore cracks remain in the substrate even after irradiation. However, in the smooth region, as a greater amount of energy is irradiated, the ablation depth becomes greater and complete removal of the cracking layer becomes possible. Additionally, the thermal diffusion depth L , or the distance a temperature change propagates within a single pulse due to thermal conduction, is estimated to be roughly $2 \mu\text{m}$ from the relation $L = (\alpha t_0)^{1/2}$ where α is thermal diffusivity and t_0 is the pulse width (Zahedi et al., 2015). As we have observed crack propagation and therefore evidence of temperature change at a greater depth, we can assume that the cumulative heating effect of multiple pulses led to an increasing ΔT .

As it is the irradiation of a single-crystal material that is being investigated, it is imperative that the effect of crystal orientation is also considered. The laser irradiation of other crystalline materials has shown that fracture mostly occurred along the natural cleavage plane (Johansen et al., 1995). Diamond normally cleaves on the (111) plane (Spriggs, 2002), thus it is expected that cracking is likely to occur along this plane. To investigate the effect of the cleavage

plane, a circular groove was irradiated using the same parameters as the other experiments and a laser fluence of 8.4 J/cm^2 , resulting in a groove as shown in Fig. 6. Upon close examination of the cracks, it was observed that the cracking direction, taken relative to the laser scanning direction, changed every 45° of the groove. As shown in Fig. 7a–c, at the point 90° from the irradiation starting point, where the laser scanning direction is perpendicular to the <100> direction, the cracks are generated at an angle to the laser scanning direction. On the other hand, as shown in Fig. 7d–f, at the point 45° from the irradiation starting point, where the laser scanning direction is perpendicular to the <110> direction, the cracks are generated perpendicular to the laser scanning direction. The cracking direction was shown to change every 45° following the same pattern. This resulted in the cracking direction being constant, regardless of laser scanning direction, thus appearing to be dependent on some inherent material property. This property could be crystal orientation and the prominent cracking direction could be along the plane (111).

All of the above experiments produced a groove with a smooth region at the center of the groove. This means that irradiation by the beam center produces a damage-free groove. Therefore, it may be possible to create damage-free grooves by employing a mask with a rectangular hole onto the irradiation surface. By irradiating the edges of the mask, the beam center can be used to form the groove edges, which will hopefully result in a damage-free rectangular groove.

3.2. Ripples formation

During laser irradiation using a single pass, the surface was either cracked or smooth. However, ripples were observed within

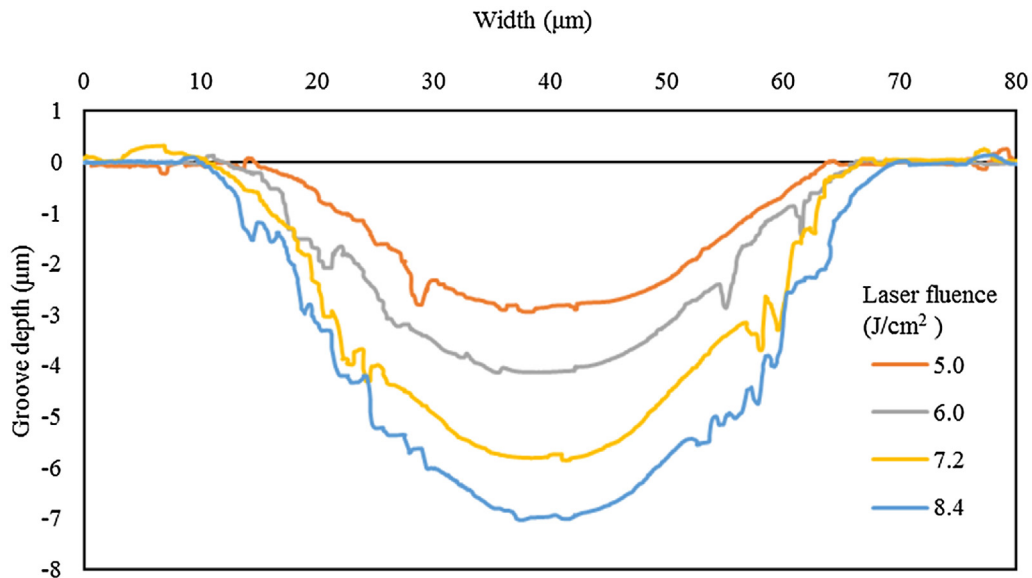


Fig. 5. Cross-sectional profile of grooves produced by varying laser fluences.

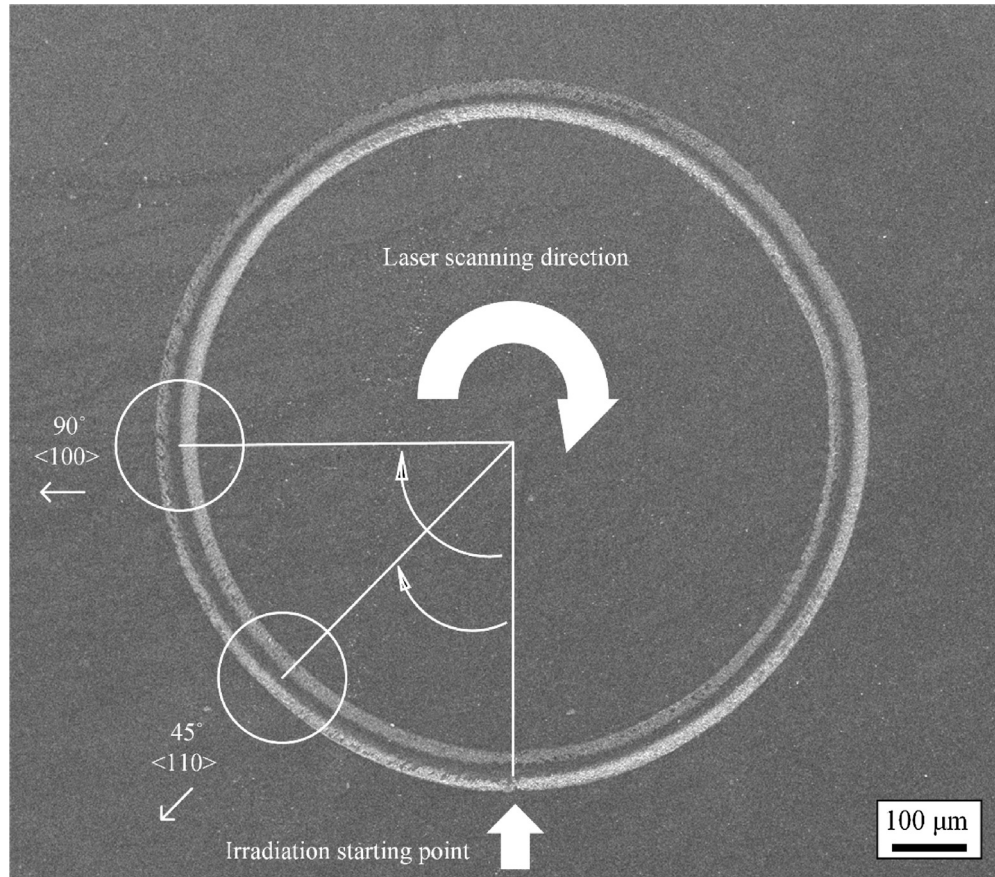


Fig. 6. SEM image of the 1 mm diameter circular groove, irradiated by a laser fluence of 8.4 J/cm². The angle, crystal orientation and observation regions are indicated.

the groove for irradiation with 5 passes and above, as indicated in Fig. 8. It is important to note here that they were only observed inside the groove; although the area outside the groove had also been irradiated, there were no ripples detected. The ripples formed were parallel to the laser scanning direction and were observed on both the groove walls and the groove bottom. The distance between

the ripples was 0.4–0.5 μm, which is close to the laser wavelength of 532 nm.

Previous studies have reported the formation of similar periodic surface structures. These are known as laser-induced periodic surface structures (LIPSS) and they are generally formed perpendicular to the incident electric field (Bonse et al., 2002). The distance between each ripple (in other words, the period of the structure)

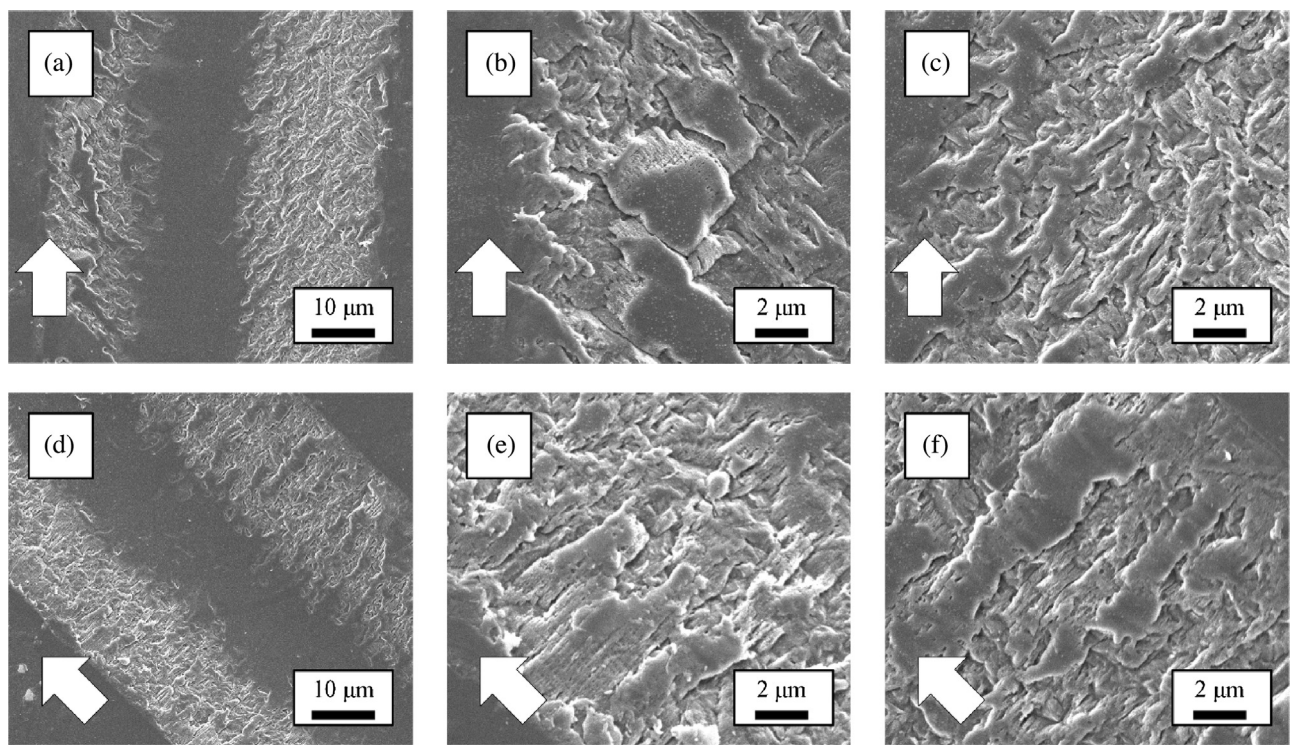


Fig. 7. SEM images of cracks formed near the edge of the circular groove at an angle of 90° or the <100> direction: (a) the entire groove, (b) the outer edge, (c) the inner edge, and of 45° or the <110> direction: (d) the entire groove, (e) the outer edge, (f) the inner edge. The laser scanning direction is shown by a white arrow.

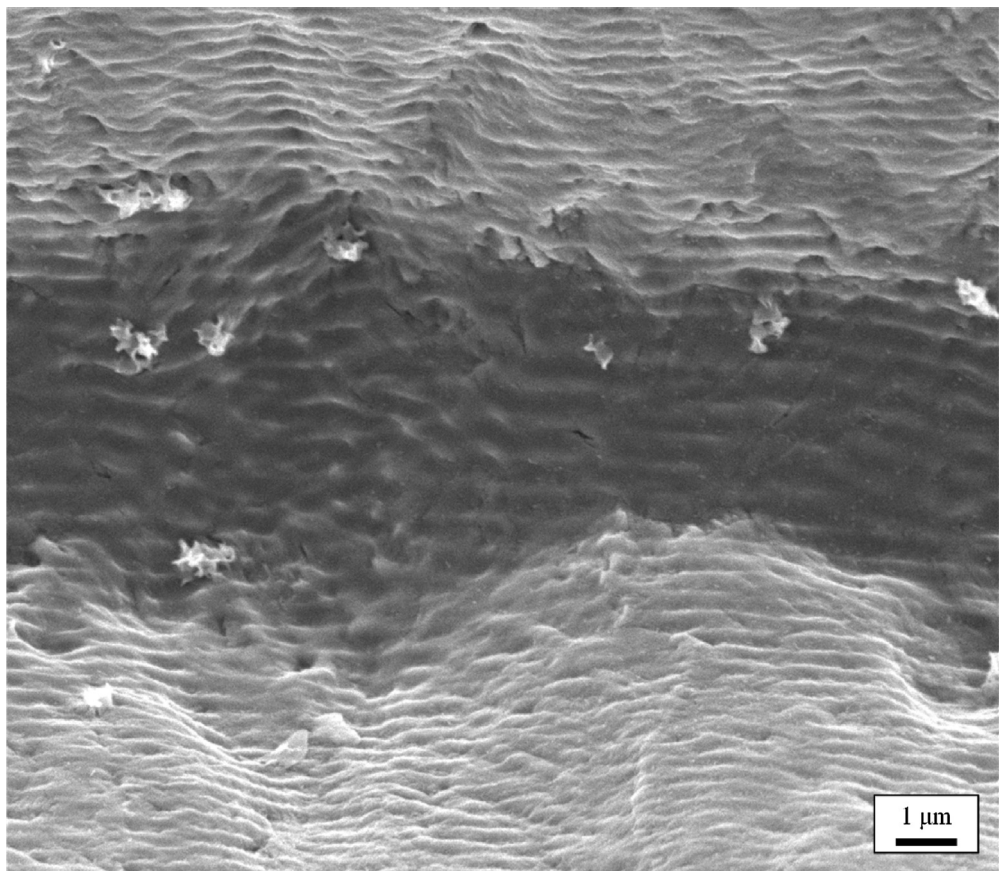


Fig. 8. Ripples observed on the groove walls and bottom produced by irradiation with 20 passes and a laser fluence of 5.0 J/cm².

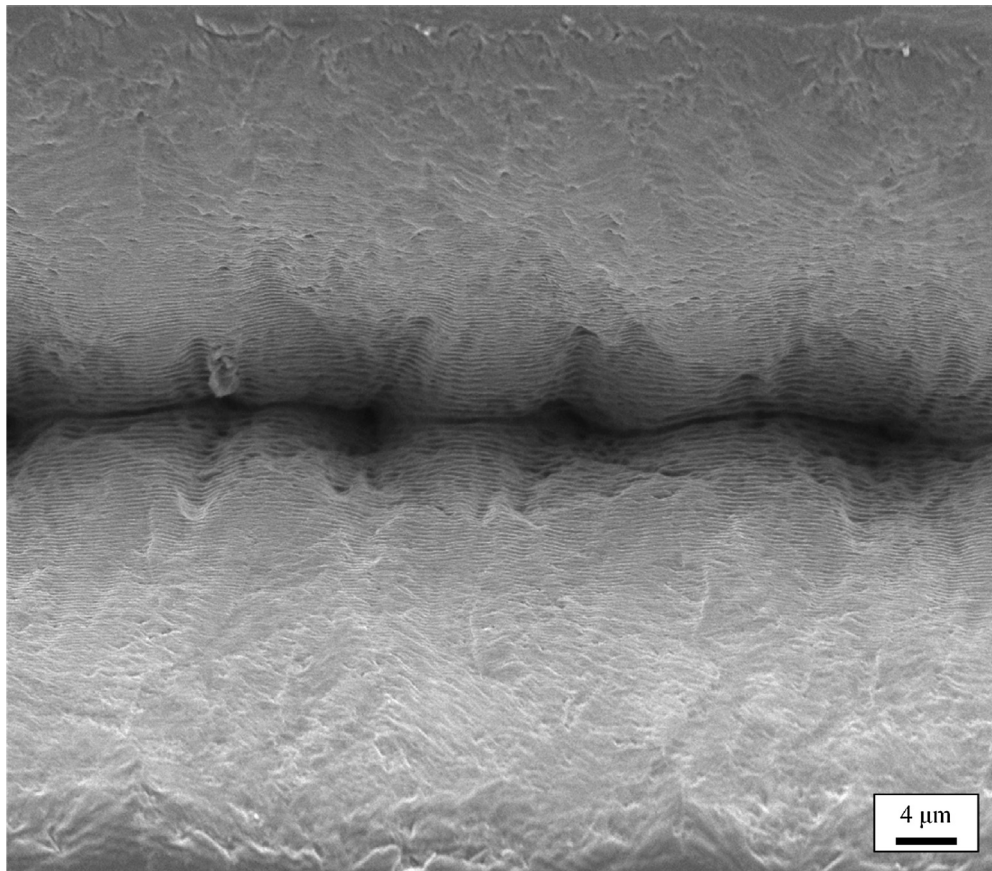


Fig. 9. SEM images of the ripples formed when diamond was irradiated using an argon stream.

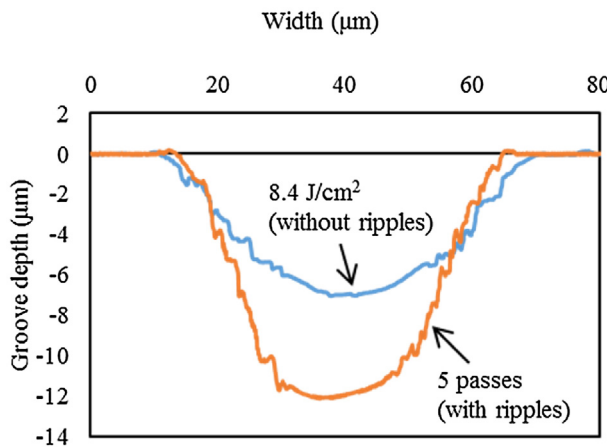


Fig. 10. Cross-sectional profile of grooves produced by 5 passes at $5.0 \text{ J}/\text{cm}^2$ and for 1 pass at $8.4 \text{ J}/\text{cm}^2$.

has been shown to be closely related to the incoming laser wavelength (Ashkenasi et al., 1998) and also the refractive index of the irradiated material (Jia et al., 2005). It is currently accepted that the LIPSS originate from the interference of the incident laser (an electromagnetic wave) with some form of surface scattered wave, experimentally demonstrated by Wu et al. (2003). However, the system in this study uses circular polarization and Guosheng et al. (1982) have mentioned that ripples are not formed when a circular polarization is used.

An alternative cause of ripple formation is the interference of the laser-induced plasma and the incoming laser beam. In order to determine whether this was the cause of these ripples, another

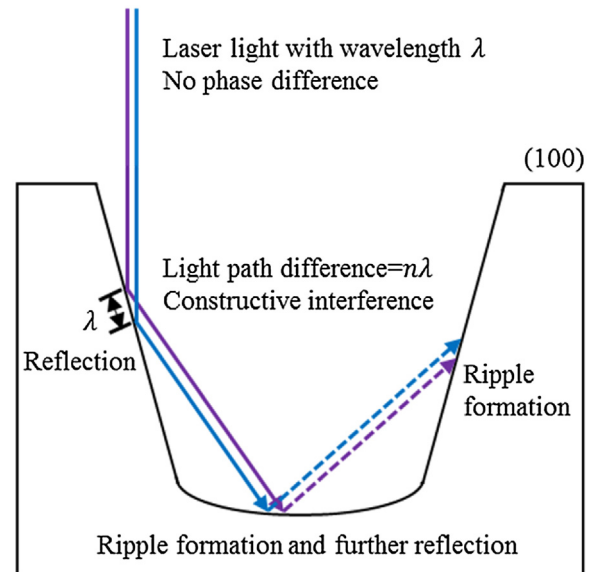


Fig. 11. Schematic for constructive interference and ripple formation.

experiment was conducted. The experiment for 50 passes was repeated using a 0.3 MPa argon gas stream in order to remove the plasma formed during irradiation. Despite the use of the gas stream, the ripples remained as shown in Fig. 9.

As the initially considered causes of the ripples were all shown to be irrelevant, ripple formation was considered in relation to groove depth. Fig. 10 presents the cross-sectional profile of the groove formed by 5 passes at $5.0 \text{ J}/\text{cm}^2$ and by 1 pass at $8.3 \text{ J}/\text{cm}^2$.

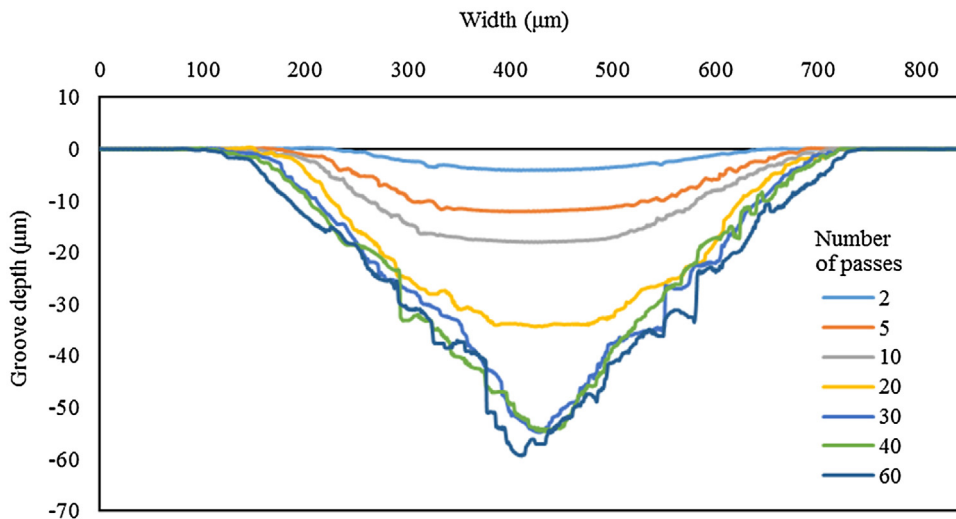


Fig. 12. Cross-sectional profile of grooves produced by a varying number of passes at $5.0\text{J}/\text{cm}^2$.

This shows that the ripples form when the groove depth is above a certain value. With a greater depth, the groove wall is steeper. When the walls are steep, the light is reflected from the groove walls and these reflected light rays interfere with each other within the groove. Mildren (2013) showed that diamond has a reflectivity of $\sim 17\%$. This interference creates an intensity distribution with a period equal to the wavelength.

To describe this process in detail, initially the groove wall is rough and can be seen to contain ripples of many different periods. However, when light is incident on and reflected from ripples with a period equal to the wavelength λ , the light path difference is equal to roughly $n\lambda$, where n is an integer. The light interferes constructively via the mechanism illustrated by Fig. 11 and the intensity reaches a maximum. The ripples with a period of λ gradually

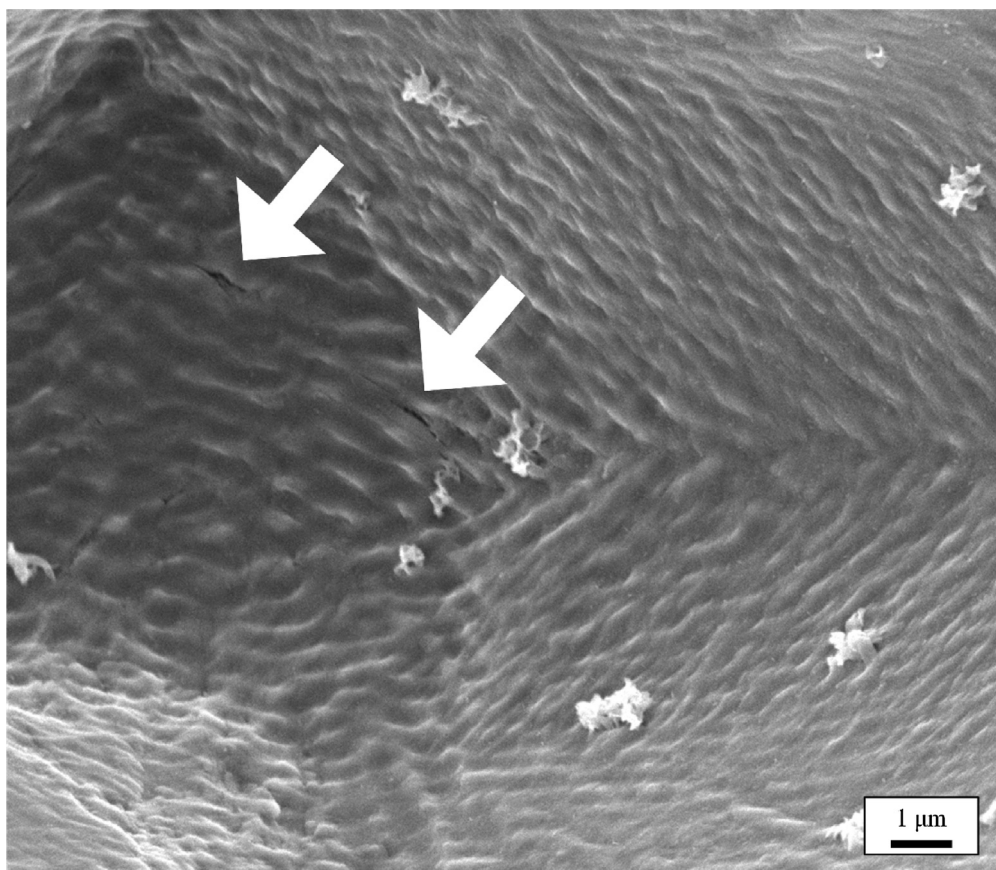


Fig. 13. The bottom of the groove produced by 20 passes at a laser fluence of $5.0\text{J}/\text{cm}^2$, where cracking is visible.

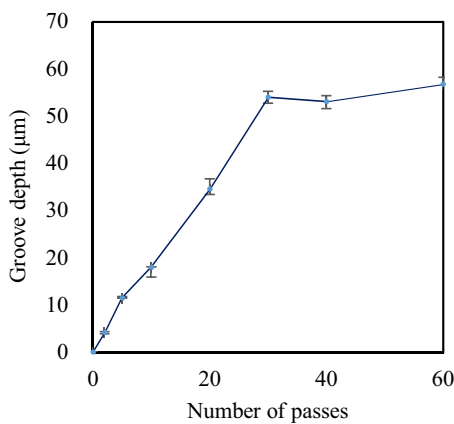


Fig. 14. Groove depth in relation to the number of passes.

become more pronounced so that ripples remain after irradiation. Thus ripples are formed when the groove walls are steep enough to cause significant internal reflection and interference. Prevention of ripple formation is possible by processing straight walls or titling the sample to prevent laser reflection.

3.3. Groove shape evolution

Fig. 12 shows the results of measuring the cross-sectional profile of the groove for irradiations with varying pass numbers. As the number of passes was increased, the groove no longer had a near-Gaussian profile. This deviation has several characteristics. Up to 10 passes, the groove was a comparatively smooth curve. At 20 passes, the groove walls became steeper but the center is still smooth. This may be because less laser energy is absorbed on a smooth surface compared to a cracked surface. Above 20 passes, the groove profile became V-shaped. The gradient of the groove walls do not change and ablation is concentrated at the groove bottom.

Some cracks are visible as in Fig. 13. Additionally, there seems to be a limit to the groove depth produced as indicated in Fig. 14. This transfer in laser-induced phenomena from material removal by ablation (20 passes and below) to crack propagation (above 20 passes) can be explained using the following mechanism. From the research of Kononenko et al. (1998), it is known that deep structures result in reduced ablation as absorption by the plasma becomes enhanced. In deep grooves, plasma movement becomes restricted and the plasma remains in the groove. It blocks further laser energy from reaching the substrate surface. Therefore, even if the diamond is irradiated with many passes, the plasma prevents further material from being ablated. Moreover, it is possible that, due to enhanced absorption, heat accumulation occurs within the plasma. Laser energy absorbed by the plasma is converted into internal energy of the plasma and radiated onto the substrate surface (Carpene et al., 2010). This heating of the surface appears to have caused increased crack propagation. To reduce shape deformation and plasma induced cracking, a single pass should be used. For a deep groove, a higher fluence may be needed.

3.4. Debris deposition

To examine debris deposition, we observed the irradiation groove before the cleaning process. Fig. 15a shows the debris deposition around the groove produced by irradiation of 20 passes. The debris formed a cloud around the groove, and from the Raman spectrum shown in Fig. 16a, the debris was identified to be disordered graphitic carbon as it exhibited a D band at 1356 cm^{-1} and a G band at 1589 cm^{-1} (Knight and White, 1989). This is a very interesting

result as, although previous studies have discussed the formation mechanism of graphite (Jeschke et al., 1999), they have not focused on the deposition of the graphitic debris cloud. As shown in Fig. 15a, the cloud contained a variety of particles. In the region closest to the groove, there were few particles. It is likely that the laser-induced plasma shielded this region from the deposition of debris particles. In an ambient gas, high plasma plume pressure drives its initial expansion as if it were occurring in a vacuum (Schou et al., 2007). Therefore this initial high pressure prevented debris deposition. As presented in Fig. 15b, only a very thin layer of extremely small (\sim submicron size) debris particles were deposited in this region. As presented in Fig. 15c, at the edge of this flat region, there were many large ($\sim 10\text{ }\mu\text{m}$) debris particles. As these particles are large, they may have been too heavy to travel any further. Beyond this wall of large particles, many small round particles were observed, shown in Fig. 15d. They appeared to be a coagulation of even smaller circular particles. As the distance from the groove increased, the particle size decreased, as indicated in Fig. 15e. The Raman spectra of these regions of debris were further examined. The shielded inner region, shown in Fig. 15b, exhibited a larger D/G intensity ratio compared to the outer region as shown in Fig. 16, indicating a greater amount of graphitic debris in the outer region. As a side note, Kuznetsov et al. (1999) stated that (100) surface of diamond requires much more atomic rearrangement to form a graphite plane compared to (111) and (110) surfaces. Thus it is possible that the results show the least laser-induced graphite out of irradiation of all other crystal planes.

It is possible that the laser-induced graphite reacted with the surrounding oxygen to produce CO_2 . This reaction occurs favorably at temperatures below the sublimation temperature of graphite. However, Rothschild et al. (1986) have found that the formation of volatile products such as CO_2 eliminated the amount of graphitic residue. As much residue was found on the machined surface, it may be concluded that not much of the graphite was chemically reacted.

Relating these observations to the cracking mechanism, it is possible to create a model representing the surface morphologies after irradiation as illustrated in Fig. 17. It is possible to divide the morphology into the following categories: a debris deposition zone, a laser unaffected zone, a cracking zone, and a smooth zone.

In addition to debris around the groove, some debris was observed inside the groove even after cleaning as presented in Fig. 18. This type of debris was small ($\sim 1\text{ }\mu\text{m}$), irregularly shaped with sharp edges and were observed for a pass number greater than 20. This may be the result of spallation, demonstrated by Körner et al. (1996), where elastically stored energy enables unstable crack growth and pieces of diamond are broken off in a violent and explosive process.

These observations enabled the identification of two types of debris produced in the irradiation of diamond. First, there were round graphitic carbon particles deposited outside of the plasma generation area. Second, they were smaller irregular diamond debris left behind inside the groove. This indicates that perhaps ablation of diamond occurs via two paths; one is the thermal graphitization of diamond and its subsequent sublimation, and the other is the direct explosive ablation of diamond, possibly during rapid, unstable crack propagation. Rothschild et al. (1986) proposed a thermal mechanism for ablation where a transformation from diamond to graphite (a highly absorbing material) occurs, followed by sublimation. However, the experimental results here suggest that diamond itself is also ablated in a mechanical process without graphitization. Graphitic debris can be removed by cleaning but to prevent the formation and deposition of diamond debris, a low pass number should be used.

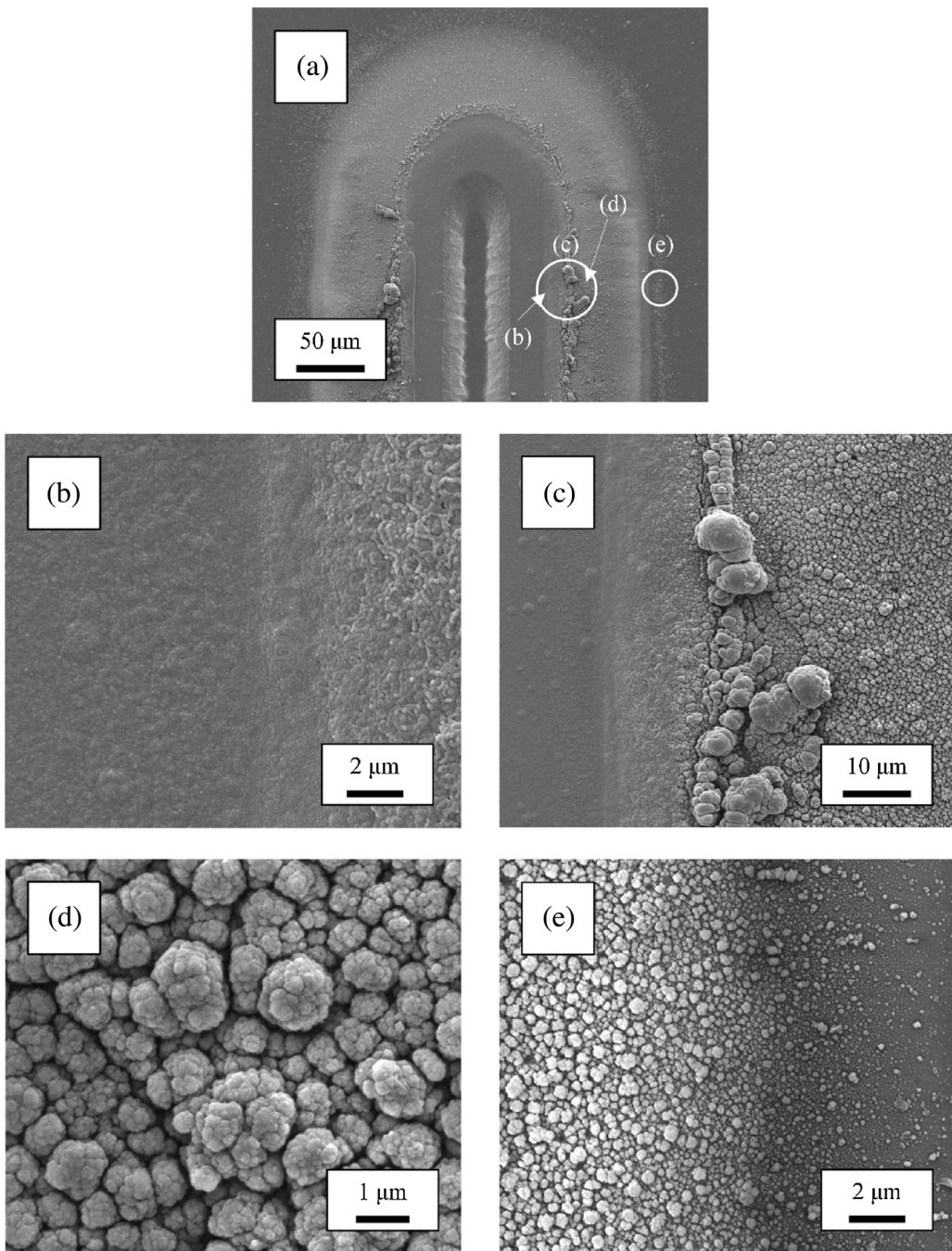


Fig. 15. SEM images of debris produced at 5.0 J/cm^2 with 20 passes: (a) the entire groove, (b) thin layer of debris deposition, (c) large debris particles, (d) small round parricles, (e) decrease in particle size.

4. Conclusion

Four types of damage have been identified in nanosecond pulsed laser irradiation on single crystal diamond. Cracking is caused by a rapid temperature change within the material. The ripples are formed by interference of the laser reflected from the groove walls. The groove shape deformation and its deviation from a Gaussian cross-section is due to enhanced absorption by the laser-

induced plasma. Finally, the deposited ablation debris is composed of two types, round graphitic carbon particles and smaller irregular diamond particles, which is indicative of two different ablation regimes. Cracking and shape deformation is reduced at the center of the groove, which is very smooth and ripple-free for line irradiations using a single pass. Graphitic debris can be easily removed by a cleaning process. These findings of the causes of laser-induced damage and the mechanism of surface formation provide useful information for development of new method for damage prevention.

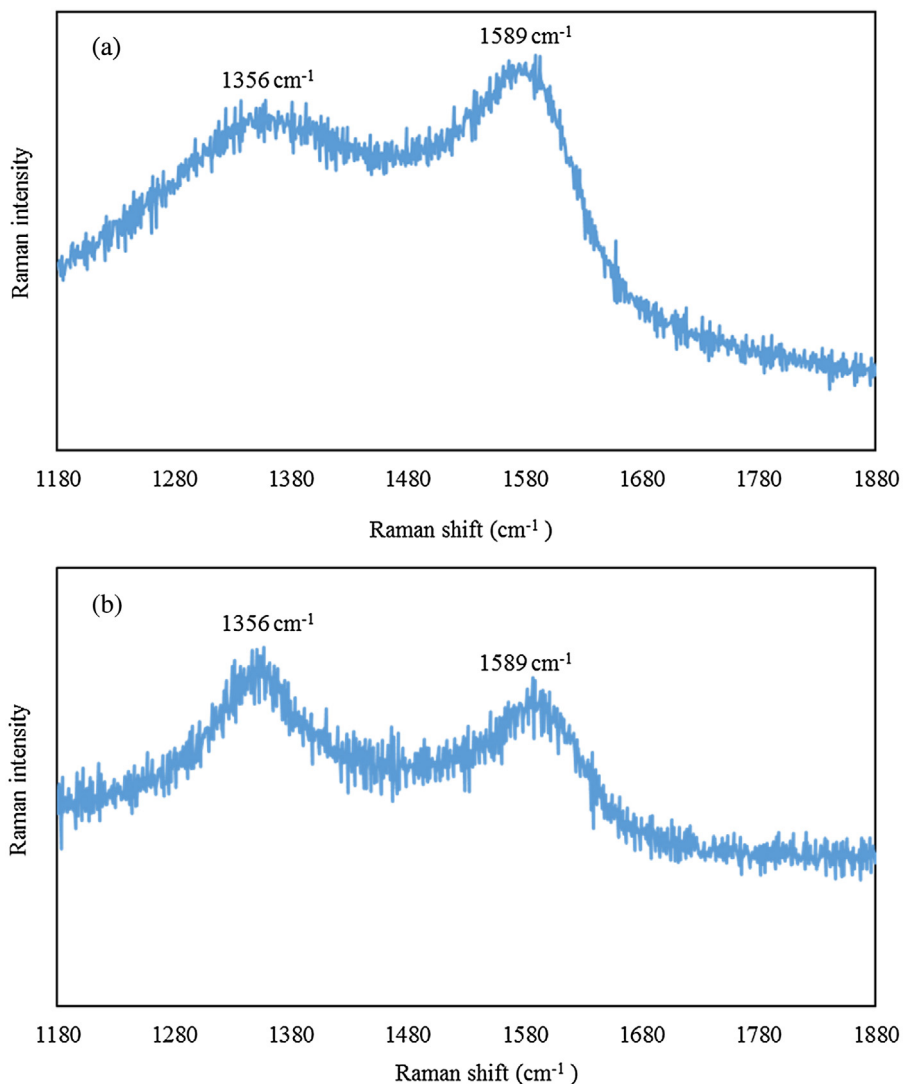


Fig. 16. Raman spectra of: (a) the debris cloud and (b) the shielded inner region, formed around the groove produced with laser irradiation with 5.0 J/cm² and 20 passes. Note that (a) shows a stronger graphite peak compared to (b).

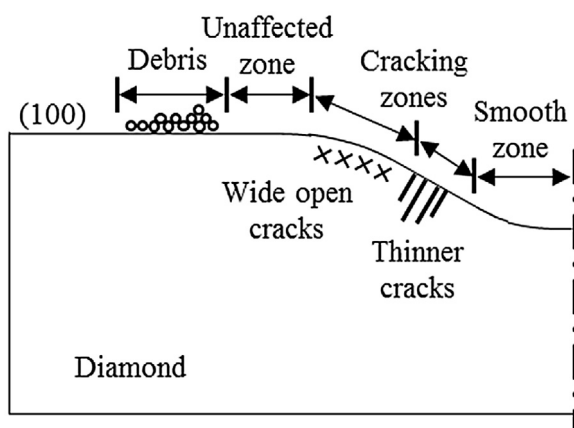


Fig. 17. Model of surface morphologies after irradiation.

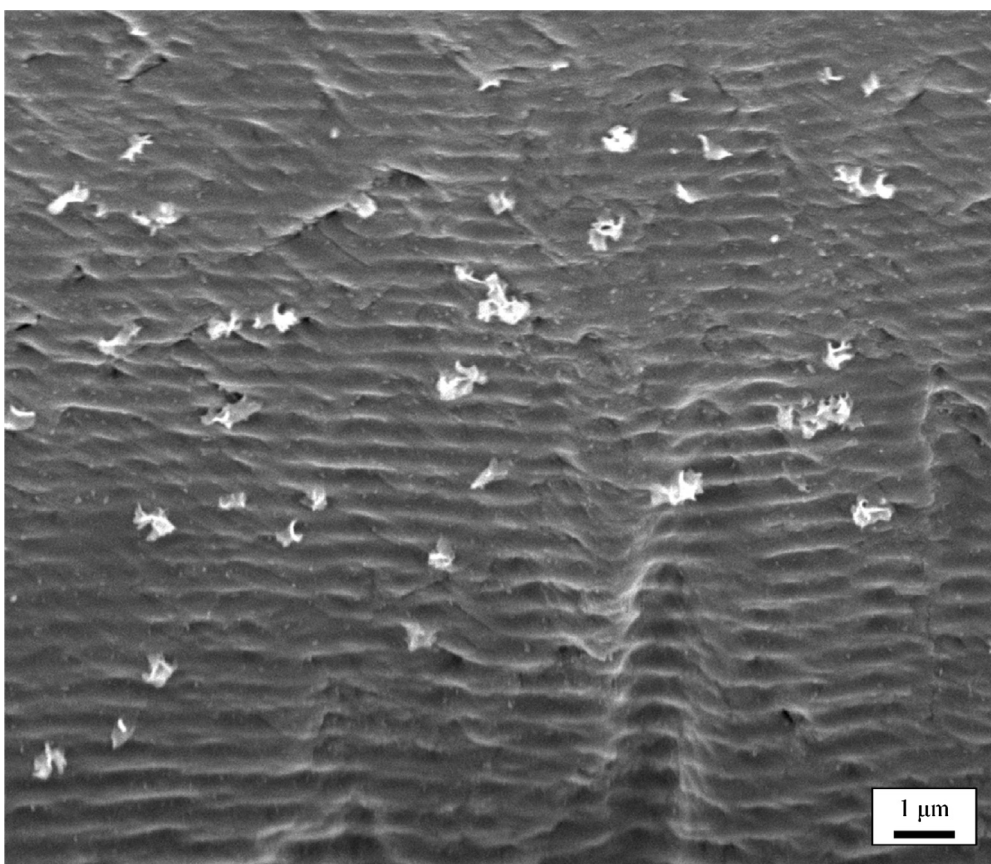


Fig. 18. Debris on the walls of the groove produced by 30 passes at a laser fluence of 5.0 J/cm^2 .

References

- Ashkenasi, D., Herbst, G., Rosenfeld, A., Varel, H., Lorenz, M., Stoian, R., Campbell, E.E.B., 1998. **Laser ablation and structuring of transparent materials with ultrashort laser pulses.** In: Phipps, C.R. (Ed.), *Proceedings of SPIE Conference on High-Power Laser Ablation 3343*. Santa Fe, New Mexico, pp. 400–410.
- Bloembergen, N., 1973. **Role of cracks, pores, and absorbing inclusions on laser induced damage threshold at surfaces of transparent dielectrics.** *Appl. Opt.* 12 (4), 661–664.
- Bonse, J., Baudach, S., Krüger, J., Kautek, W., Lenzner, M., 2002. **Femtosecond laser ablation of silicon-modification thresholds and morphology.** *Appl. Phys. A* 74 (1), 19–25.
- Carpene, E., Höche, D., Schaaf, P., 2010. **Fundamentals of laser-material interactions.** In: Schaaf, P. (Ed.), *Laser Processing of Materials: Fundamentals, Applications and Developments*, vol. 139. Springer Berlin, Heidelberg, Berlin, pp. 39–40.
- Chichkov, B.N., Momma, C., Nolte, S., von Alvensleben, F., Tünnermann, A., 1996. **Femtosecond, picosecond and nanosecond laser ablation of solids.** *Appl. Phys. A* 63 (2), 109–115.
- Dumitru, G., Romano, V., Weber, H.P., Sentis, M., Marine, W., 2002. **Femtosecond ablation of ultrahard materials.** *Appl. Phys. A* 74 (6), 729–739.
- Eberle, G., Jefimovs, K., Wegener, K., 2015. **Characterisation of thermal influences after laser processing polycrystalline diamond composites using long to ultrashort pulse durations.** *Precis. Eng.* 39, 16–24.
- Fassai, A.Y., Mwenifumbo, S., Rahbar, N., Chen, J., Li, M., Beye, A.C., Arnold, C.B., Soboyejo, W.O., 2009. **Nano-second UV laser processed micro-grooves on Ti6Al4V for biomedical applications.** *Mater. Sci. Eng. C* 29 (1), 5–13.
- Feit, M.D., Rubenchik, A.M., 2004. **Influence of subsurface cracks on laser induced surface damage.** In: Exarhos, G.J., Guenther, A.H., Kaiser, N., Lewis, K.L., Soileau, M.J., Stoltz, C.J. (Eds.), *Proceedings of SPIE*. Vol. 5273 Bellingham, WA, USA, pp. 264–272.
- Frenkel, S.R., Simon, J., Alexander, H., Dennis, M., Ricci, J.L., 2002. **Osseointegration on metallic implant surfaces: effects of microgeometry and growth factor treatment.** *J. Biomed. Mater. Res.* 63 (6), 706–713.
- Guosheng, Z., Fauchet, P.M., Siegman, A.E., 1982. **Growth of spontaneous periodic surface structures on solids during laser illumination.** *Phys. Rev. B* 26 (10), 5366–5381.
- Hasselman, D.P.H., 1969. **Unified theory of thermal shock fracture initiation and crack propagation in brittle ceramics.** *J. Am. Ceram. Soc.* 52 (11), 600–604.
- Jeschke, H.O., Garcia, M.E., Bennemann, K.H., 1999. **Theory for laser-induced ultrafast phase transitions in carbon.** *Appl. Phys. A* 69 (1), S49–S53.
- Jia, T.Q., Chen, H.X., Huang, M., Zhao, F.L., Qiu, J.R., Li, R.X., Xu, Z.Z., He, X.K., Zhang, J., Kuroda, H., 2005. **Formation of nanogratings on the surface of a ZnSe crystal irradiated by femtosecond laser pulses.** *Phys. Rev. B* 72 (12), 1–4 (125429).
- Johansen, H., Gogoll, S., Stenzel, E., Reichling, M., Matthias, E., 1995. **SEM-analysis of fracture features formed in excimer-laser induced surface damage of CaF₂.** *Radiat. Eff. Defects Solids* 136, 151–156.
- Körner, C., Mayerhofer, R., Hartmann, M., Bergmann, H.W., 1996. **Physical and material aspects in using visible laser pulses of nanosecond duration for ablation.** *Appl. Phys. A* 63 (2), 123–131.
- Kawasegi, N., Sugimori, H., Morimoto, H., Morita, N., Hori, I., 2009. **Development of cutting tools with microscale and nanoscale textures to improve frictional behavior.** *Precis. Eng.* 33 (3), 248–254.
- Knight, D.S., White, W.B., 1989. **Characterization of diamond films by Raman spectroscopy.** *J. Mater. Res.* 4 (2), 385–393.
- Kononenko, T.V., Ralchenko, V.G., Vlasov, I.I., Garnov, S.V., Konov, V.I., 1998. **Ablation of CVD diamond with nanosecond laser pulses of UV–IR range.** *Diam. Relat. Mater.* 7 (11), 1623–1627.
- Kononenko, V.V., Kononenko, T.V., Pimenov, S.M., Sinyavskii, M.N., Konov, V.I., Dausinger, F., 2005. **Effect of the pulse duration on graphitisation of diamond during laser ablation.** *Quantum Electron.* 35 (3), 252–256.
- Konov, V.I., 2012. **Laser in micro and nanoprocessing of diamond materials.** *Laser Photonics Rev.* 6 (6), 739–766.
- Korin, N., Bransky, A., Khouri, M., Dinnar, U., Levenberg, S., 2009. **Design of well and groove microchannel bioreactors for cell culture.** *Biotechnol. Bioeng.* 102 (4), 1222–1230.
- Kuznetsov, V.L., Zilberman, I.L., Butenko, Y.V., Chuvilin, A.L., Segall, B., 1999. **Theoretical study of the formation of closed curved graphite-like structures during annealing of diamond surface.** *J. Appl. Phys.* 86 (2), 863–870.
- Lee, Y., 2011. **Evaluating subsurface damage in optical glasses.** *J. Eur. Opt. Soc.—Rapid Publ.* 11001, 1–11.
- Mildren, R.P., 2013. **Intrinsic optical properties of diamond.** In: Mildren, R.P., Rabeau, J.R. (Eds.), *Optical Engineering of Diamond*. Wiley-VCH Verlag GmbH & Co, Weinheim, Germany, pp. 1–3.
- Obikawa, T., Kamio, A., Takaoka, H., Osada, A., 2011. **Micro-texture at the coated tool face for high performance cutting.** *Int. J. Mach. Tool Manuf.* 51 (12), 966–972.
- Preuss, S., Stuke, M., 1995. **Subpicosecond ultraviolet laser ablation of diamond: nonlinear properties at 248 nm and time-resolved characterization of ablation dynamics.** *Appl. Phys. Lett.* 67 (3), 338–340.

- Rothschild, M., Arnone, C., Ehrlich, D.J., 1986. Excimer-laser etching of diamond and hard carbon films by direct writing and optical projection. *J. Vac. Sci. Technol. B* 4 (1), 310–314.
- Sack, R.A., 1946. Extension of Griffith's theory of rupture to three dimensions. *Proc. Phys. Soc.* 58 (6), 729–736.
- Schou, J., Amoruso, S., Lunney, J.G., 2007. Plume dynamics. In: Phipps, C. (Ed.), *Laser Ablation and Its Applications, vol 129*. Springer Science+Business Media LLC, New York, pp. 81–83.
- Stuart, B.C., Feit, M.D., Herman, S., Rubenchik, A.M., Shore, B.W., Perry, M.D., 1996. Nanosecond-to-femtosecond laser-induced breakdown in dielectrics. *Phys. Rev. B* 53 (4), 1749–1761.
- Sugihara, T., Enomoto, T., 2009. Development of a cutting tool with a nano/micro-textured surface-improvement of anti-adhesive effect by considering the texture patterns. *Precis. Eng.* 33 (4), 425–429.
- Wilkinson, C.D.W., Riehle, M., Wood, M., Gallagher, J., Curtis, A.S.G., 2002. The use of materials patterned on a nano- and micro-metric scale in cellular engineering. *Mater. Sci. Eng. C* 19 (1), 263–269.
- Wu, Q., Ma, Y., Fang, R., Liao, Y., Yu, Q., Chen, X., Wang, K., 2003. Femtosecond laser-induced periodic surface structure on diamond film. *Appl. Phys. Lett.* 82 (11), 1703–1705.
- Yan, J., Oowada, T., Zhou, T., Kuriyagawa, T., 2009. Precision machining of microstructures on electroless-plated NiP surface for molding glass components. *J. Mater. Proc. Tech.* 209 (10), 4802–4808.
- Zahedi, A., Tawakoli, T., Azarhoushang, B., Akbari, J., 2015. Picosecond laser treatment of metal-bonded CBN and diamond superabrasive surfaces. *Int. J. Adv. Manuf. Technol.* 76 (5), 1479–1491.